Unidirectional spin wave propagation due to a saturation magnetization gradient

P. Borys [1,2,*] O. Kolokoltsev [1] N. Qureshi [1] M. L. Plumer [2,3] and T. L. Monchesky [2]

[1] *Instituto de Ciencias Aplicadas y Tecnología, Universidad Nacional Autónoma de México, Ciudad Universitaria 04510, Mexico*

[2] *Department of Physics and Atmospheric Science, Dalhousie University, Halifax, Nova Scotia B3H 4R2, Canada*

[3] *Department of Physics and Physical Oceanography, Memorial University of Newfoundland, St. John's, Newfoundland and Labrador A1B 3X7, Canada*

(Received 8 December 2020; revised 18 March 2021; accepted 24 March 2021; published 7 April 2021)

We demonstrate using micromagnetic simulations and a theoretical model that a gradient in the saturation magnetization (M_s) of a perpendicularly magnetized ferromagnetic film induces a nonreciprocal spin-wave propagation and, consequently, an asymmetric dispersion relation. The M_s gradient adds a linear potential to the spin-wave equation of motion consistent with the presence of a force. We consider a transformation from an inertial reference frame in which the M_s is constant to an accelerated reference frame where the resulting inertial force corresponds to the force from the M_s gradient. As in the Doppler effect, the frequency shift leads to an asymmetric dispersion relation. We show that under certain circumstances, unidirectional propagation of spin waves can be achieved, which is essential for the design of magnonic circuits. Our results become more relevant in light of recent experimental works in which a suitable thermal landscape is used to dynamically modulate the saturation magnetization.

DOI: 10.1103/PhysRevB.103.144411

I. INTRODUCTION

Magnonics, the field that studies the behavior of spin waves and their quanta magnons, has received much attention as a plausible complement to conventional semiconductor electronics, mainly because data transport and processing occurs free of any flow of charge and hence free of the undesired Joule heating [1–7]. For magnonic devices to be of practical relevance there are several challenges to overcome including: more advances in material science to develop new magnetic media with low damping and control over the magnetic parameters; magnon manipulation by electric currents and electric fields to allow a merging with electronics; dynamical modulation of the magnetic parameters using heat; and miniaturization of the magnonic devices leading to an increase in the operating frequency [8–11]. As miniaturization to the nanoscale is achieved, spin waves are described primarily by the exchange interaction and while exchange spin waves have been detected using spin-polarized electron energy loss spectroscopy (SPEELS) for over 20 years [12–14], it was only recently that excitation and confinement of exchange spin waves, specially in low-damping YIG films, was finally realized opening a wide range of technological paths [15–18]. Contrary to long wavelength, magnetostatic-dominated spin waves that can exhibit nonreciprocal propagation, short-wavelength spin waves are isotropic in their propagation due to the isotropic nature of the exchange interaction, dominant at this scale. Several mechanisms have been proposed to make the dispersion asymmetric since anisotropic propagation is key to the design of magnonic circuitry. Examples of such mechanisms include induced Dzyaloshinskii-Moriya interaction [19–25], dipolar coupling [26–28], and an external magnetic field [29]. Following the ideas behind graded-index optics, a continuous modulation of the magnetic parameters has been recently proposed to control spin-wave propagation [30–34]. For example, it has been shown that a gradual modulation of the saturation magnetization (M_s) created with thermal landscapes can steer spin waves and change their dispersion relation as they propagate [35–40].

In this work, we use micromagnetic simulations to demonstrate that exchange spin waves do not propagate reciprocally in a perpendicularly magnetized ferromagnetic thin film in which M_s varies linearly along the length of the film. To understand the origin of the phenomenon, we solve the linearized Landau-Lifshitz (LL) equation of motion analytically. The linear variation in M_s along the x direction creates an effective linear potential $V(x)$ in the spin-wave equation of motion. We transform to a noninertial frame of reference where the inertial force cancels the force associated with the linear spin-wave potential and allows the LL equation to be solved in the familiar constant M_s condition. However, when we transform back to the inertial frame, there is a frequency shift due to the acceleration of the excitation source similar to what happens in the Doppler effect that broadens the spin-wave dispersion. It is this Doppler shift of the spin waves that is the origin of the nonreciprocal behavior.

II. RESULTS AND DISCUSSION

A. Simulations

Using GPU-accelerated, micromagnetic code Mumax3 [41], we considered a 20 μm $\times$ 256 nm $\times$ 1 nm film

*pabloborys@ciencias.unam.mx

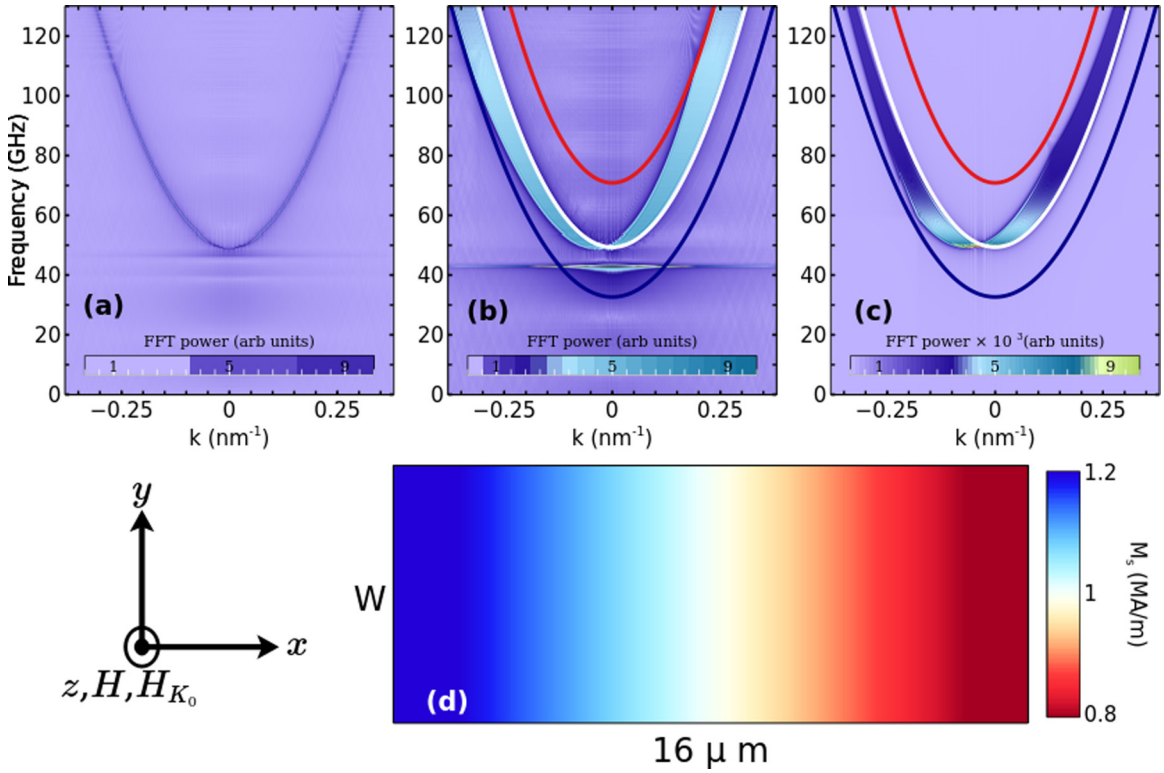

FIG. 1. (a), (b) Dispersion curves found from micromagnetic simulations in the constant M_s and gradient M_s case, respectively. In (b) solid lines represent the theoretical dispersions calculated using M_s values at the edges and in the middle of the film. (c) Dispersion curve obtained from the theoretical model with corresponding theoretical curves for comparison with (b). (d) M_s linear gradient in the film used in the simulation. The coordinate system shows the direction of the applied magnetic field $\mathbf{H}$ and the anisotropy effective field $\mathbf{H}_{\mathbf{K_0}}$. Note that the FFT power units in (c) is three orders of magnitude larger than (a) and (b) as Airy functions are not square-integrable and hence non-normalizable.

discretized using 10000 × 128 × 1 finite difference cells. Periodic boundary conditions were used along the y direction so that the effective width was 5376 nm. We used magnetic parameters of materials with perpendicular magnetic anisotropy such as Pt/CoFeB [42]: exchange constant $A = 15$ pJ/m, uniaxial anisotropy $K_u = 1$ MJ/m^3, and a magnetic field applied in the $\hat{\mathbf{z}}$ direction with a magnitude of $\mu_0 H = 1$ T, and recorded $m_y(x,t)$ in response to a field excitation of the form $h_0 \mathrm{sinc}(2\pi f_c t)\hat{\mathbf{y}}$ with $\mu_0 h_0 = 50$ mT and cutoff frequency $f_c = 500$ GHz applied along the width over one cell in the x direction positioned at the center of the film $x = 0$. Damping was not included in any simulation throughout this work. The dispersion curve is obtained by performing a fast Fourier transform (2D-FFT) on $m_y(x,t)$ to get $m_y(k,\omega)$ [43,44]. We first considered a constant saturation magnetization $M_0 = 1$ MA/m throughout the sample and show the dispersion as a surface plot of $m_y(k,\omega)$ in Fig. 1(a). The dispersion curve exhibits the typical exchange-driven quadratic form, $\omega_c \propto k^2$, in which spin waves propagating to the right and to the left have the same frequency. The magnetization gradient was modeled by a linear variation of M_s across 250 regions in the range $x = [-8\ \mu\mathrm{m}, 8\ \mu\mathrm{m}]$ [see Fig. 1(e)]. The maximum value $M_s(-8\,\mu\mathrm{m}) = 1.2$ MA/m, and minimum value $M_s(8\,\mu\mathrm{m}) = 0.8$ MA/m may be achieved in Pt/CoFeB by creating a suitable thermal landscape [42]. In Fig 1(b), we show the dispersion curve obtained for spin waves propagating in a film with a M_s gradient; additionally, solid lines indicate the theoretical dispersions corresponding to the M_s values at the edges and the middle of the film. There is a horizontal line below the ferromagnetic resonance at 41 GHz related to a strong spin-wave localization at the samples edges due to the formation of a potential well in an inhomogeneous internal magnetic field [45]. Two features contrast the constant M_s case: First, there is an asymmetry in the dispersion curve with respect to $k = 0$. Second, the dispersion curve is significantly broadened. For positive (negative) propagation, $k > 0$ ($k < 0$), as the absolute value of k increases, the broadening extend from the 1 MA/m curve, white solid line, towards the 0.8 MA/m red (1.2 MA/m blue) solid line.

B. Analytical model

To understand the dispersion curve, we construct an analytical model of the spin-wave propagation in an uniaxial ferromagnetic film with magnetic energy,

$$E = \int dV\, A(\nabla \mathbf{m})^2 - K_0\, m_z^2 - \mu_0 H M_s m_z, \qquad (1)$$

where $K_0 = K_u - \mu_0 M_s^2/2$ is the effective anisotropy including the perpendicular demagnetizing field in the local approximation and $m = (m_x, m_y, m_z)$ is a unit vector pointing in the direction of the magnetization $\mathbf{M}$. We are interested in the dynamic behavior of the spin-wave fluctuations $\delta\mathbf{m}(\mathbf{x},t)$, around the static configuration, $\mathbf{m}_0 = m_z$. To obtain the equations of motion in the long-wavelength limit we use

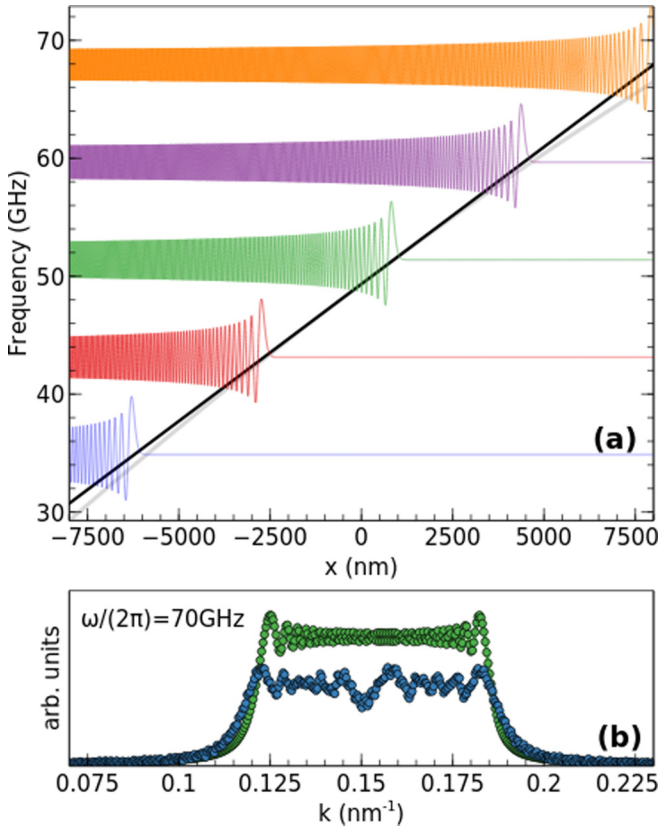

FIG. 2. Stationary solutions. In (a) the solution for five different frequencies are presented, the black solid line corresponds to the potential considered for the theoretical calculations, while the light gray curve is the complete potential $\omega_0 + qx + \gamma\mu_0(\alpha x)^2/M_0$. In (b) we present the k profile of the stationary solutions together with $m_y(k, t_0)$ from simulations for comparison.

$\mathbf{m}(\mathbf{x}, t) = m_z + \delta\mathbf{m}(\mathbf{x}, t)$ to linearize

$$\frac{\partial \mathbf{m}}{\partial t} = -\gamma \mathbf{m} \times \left(-\frac{1}{M_s}\frac{\delta E}{\delta \mathbf{m}}\right), \tag{2}$$

which can be cast as

$$i\frac{\partial}{\partial t}m_+ = \gamma\left[-\frac{2A}{M_s}\frac{\partial^2}{\partial_x^2} + \frac{2K_0}{M_s} + \mu_0 H\right]m_+, \tag{3}$$

for circularly polarized waves, $m_+ = \delta m_x + i\delta m_y$. The saturation magnetization varies linearly as $M_s(x) = M_0 + \alpha x$, which converts Eq. (3) to

$$i\frac{\partial}{\partial_t}m_+ = \left[-\frac{1}{2\beta}\frac{\partial^2}{\partial_x^2} + \omega_0 + q'x - \frac{\gamma\mu_0}{M_0}(\alpha x)^2 - i\frac{\alpha x}{M_0}\frac{\partial}{\partial_t}\right]m_+, \tag{4}$$

where we have defined the effective mass $\beta = M_0/(4\gamma A)$, the effective potential $\omega_0 = \gamma(2K_0/M_0 + \mu_0 H - \mu_0 M_0)$, and $q' = \gamma\mu_0\alpha(H - 2M_0)/M_0$ related to the force that the magnetization gradient exerts on the spin waves. Equation (4) is a Schrödinger-like equation where the term quadratic in x slightly modifies the linear potential and will be neglected (see Fig. 2 where the soft gray curve shows the effect of considering this term). The last term couples the space and time coordinates, and in order to continue with an analytical description, we replace the time derivative in this term with the lowest possible spin-wave frequency, the ferromagnetic resonant frequency, ω_0. Then the equation to solve is

$$i\frac{\partial}{\partial_t}m_+ = \left(-\frac{1}{2\beta}\frac{\partial^2}{\partial_x^2} + \omega_0 + qx\right)m_+, \tag{5}$$

where $q = \gamma\mu_0\alpha/M_0(H - 2M_0 - \omega_0/\gamma\mu_0) = -\alpha\gamma\mu_0(1 + 2K_u/\mu_0 M_0^2)$. It is worth noting the importance of the space-time coupled term, without it $q = \gamma\mu_0\alpha/M_0(H - 2M_0)$, which would allow a change of sign for $H > 2M_0$ and a fixed α value. The coupled term prevents the unphysical situation where the sign of q is not determined entirely by α.

From the dispersion curve in Fig. 1(b), it is clear that a function of the form $\omega(k)$ is not achievable in the presence of a magnetization gradient. To obtain an analytical description of the dispersion we perform a Fourier analysis of the solutions $m_+(x, t)$ to Eq. (5). We start with the Landau-Lifshitz equation that describes the spin waves in a perpendicularly magnetized magnetic film with a constant M_s throughout the film,

$$\left(-\frac{1}{2\beta}\frac{\partial^2}{\partial x'^2} + \omega_0\right)n_+ = i\frac{\partial}{\partial t'}n_+, \tag{6}$$

where $n_+(x', t') = n_x + in_y$, n_x and n_y are spin-wave components, and the dispersion can be calculated to be $\omega_c(k) = 1/(2\beta)k^2 + \omega_0$. We then transform Eq. (6) into an accelerated system described by $x = x' - 1/2(q/\beta)t'^2$ and $t' = t$ with the acceleration of the system given by $-q/\beta$. Under this transformation, the derivatives are $\partial_x' = \partial_x$ and $\partial_t' = \partial_t - (qt/\beta)\partial_x$, so that the equation in the accelerated reference frame is

$$-\frac{1}{2\beta}\frac{\partial^2}{\partial x^2}n_+ + \omega_0 n_+ + i\frac{qt}{\beta}\frac{\partial}{\partial x}n_+ = i\frac{\partial}{\partial t}n_+. \tag{7}$$

Equation (7) rightly describes the spin waves in the transformed system. However, to an observer at rest in the accelerated reference frame, there should be a potential of the form fx where f is the inertial force producing the acceleration $-q/\beta$ instead of the coupled term $i(qt/\beta)\partial_x n_+$. Following Refs. [46–49] we perform a unitary transformation

$$n_+(x', t') = m_+(x, t)e^{iqtx}e^{iq^2t^3/(6\beta)}, \tag{8}$$

where $m_+(x, t)$ obeys Eq. (5) and effectively represents the physical situation with the potential qx included.

The stationary solution to Eq. (5),

$$Ai[(2\beta q)^{1/3}(x - x_0)]e^{-i\omega t} = Ai[B\xi]e^{-i\omega t} \tag{9}$$

is an Airy function with $x_0 = (\omega - \omega_0)/q$, and is presented in Fig. 2(a) for five different frequencies $f = \omega/(2\pi)$. In Fig. 2(b) we present the k profile for the stationary solution with $f = 70\,\mathrm{GHz}$ and compare with data obtained from a simulation in which the excitation field is of the form $h_0 \sin(2\pi f_c t)\hat{\mathbf{y}}$ with $\mu_0 h_0 = 50\,\mathrm{mT}$ and frequency $f = 70\,\mathrm{GHz}$. As a result of the M_s gradient, one frequency excites a band of wave numbers, which in turn broadens the dispersion relation.

Using the stationary solution together with the integral representation of the Airy function,

$$Ai[B\xi]e^{-i\omega(k)t} = \frac{1}{2\pi B}\int_{-\infty}^{\infty} dk \exp\left[i\left(\frac{k^3}{3B^3} + k\xi - \omega(k)t\right)\right], \tag{10}$$

it is possible to construct an Airy wave packet. While we do not know $\omega(k)$ in the accelerated system, we can transform back to the primed, inertial, reference frame in which $\omega(k) = \omega_c(k) = 1/(2\beta)k^2 + \omega_0$ to calculate the integral,

$$\frac{e^{-iqt(x'-qt'^2/2\beta)}e^{-iq^2t'^3/6\beta}e^{-i\omega_0 t'}}{2\pi B}\int_{-\infty}^{\infty} dk \exp\left[i\left(\frac{k^3}{3B^3} + k\xi' - \frac{k^2 t'}{2\beta}\right)\right], \tag{11}$$

using the useful formula $\int_{-\infty}^{\infty} du\ \exp[i(u^3/3 + su^2 + ru)] = 2\pi e^{is(2s^2/3-r)}Ai(r - s^2)$. After transforming back to the accelerated system, the Airy wave packet becomes

$$m_+(x,t) = e^{-iqtx}e^{-iq^2t^3/6\beta}e^{-i\omega_0 t}Ai\left[B\left(x + \frac{qt^2}{2\beta}\right) - \left(\frac{B^2 t}{2\beta}\right)^2\right]e^{-iB^2t/(2\beta)(B^4t^2/(6\beta^2) - B(x+\frac{qt^2}{2\beta}))}. \tag{12}$$

Substitution of Eq. (12) in Eq. (5) verifies it is a solution. Figure 1(c) shows the FFT of $m_+(x,t)$ obtained from Eq. (12) and displays a good agreement with the dispersion curve obtained from the micromagnetic simulation, Fig 1(b). In particular, the asymmetry and limits of the dispersion curve match. For higher frequencies our theoretical model appears narrower compared to the simulations. This is because of the approximation made on the space-time coupled term [Eq. (4)]. To visualize the accelerated reference frame and to compare the theoretical and simulated accelerations, we change the place of excitation from the middle to the right edge of the film and record $m_y(x,t)$ for the gradient and constant M_s situations. Figure 3(a) shows the recorded data for the M_s gradient case and the solid white line corresponds to the position of the front wave in the constant M_s case. The spin waves propagating in the M_s gradient appear to be accelerated in the negative direction. The transformations are $x = x' - 1/2(q/\beta)t'^2$, $t = t'$ where (x,t) are the coordinates in the accelerated frame, and (x',t') are the coordinates in the inertial system. The point $x = 0$ corresponds to $x' = 1/2(q/\beta)t'^2$ so that the accelerated frame is moving in the $1/2(q/\beta)t'^2$ direction. An observer in the accelerated frame should feel an inertial force in the $-1/2(q/\beta)t'^2$ direction producing an acceleration $(-q/\beta) = -1.55 \times 10^{11}$ m/s^2 with the parameters used in the simulations. In Fig. 3(b), we show the difference between the front waves of spin propagating in the accelerated frame and in the inertial frame as a function of time. After fitting the curve we find that $\Delta x(t) = 1/2a(t - t_0)^2 - \Delta x_0$ with an acceleration $a = -7.52 \times 10^{11}$ m/s^2 and a time $t_0 = 1.40$ ns at which the maximum separation in the front waves $\Delta x_0 = 0.76$ μm is reached. The theoretical acceleration q/β is lower than a by a factor of five, which is attributable to the two approximations being made, namely, the quadratic term in x in the potential that was neglected, and the space-time coupled term that was replaced with the lowest possible frequency ω_0. Still, the theoretical and simulated dispersion curves show a good agreement and the spin-wave acceleration is clear.

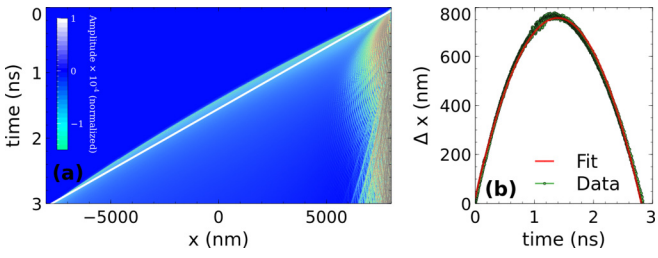

FIG. 3. Spin-wave acceleration. (a) Micromagnetic simulation of spin waves excited at the right edge of the M_s gradient at $t = 0$, the white solid lines represents the trajectory the front wave follows in the M_s constant case. In (b) we present the absolute difference Δx between the front wave position in the M_s gradient case and the front wave position in the M_s constant case as a function of time. The red solid line corresponds to the fitting.

C. Doppler effect

The transformation of Eq. (6) into Eq. (5) is the key concept of the analytical description above. It demonstrates that a system with a saturation magnetization gradient is equivalent to a system with a constant saturation magnetization being accelerated with respect to an inertial or laboratory reference frame. Our model shifts from a description in which all effective fields in the equation of motion are spatially inhomogeneous to a simplified description in an accelerated frame where all magnetic parameters are constant. We now discuss the physical mechanism of the nonreciprocal dispersion from the point of view of the Doppler effect. According to our model, a thin ferromagnetic film with constant M_s accelerates to the right with respect to the laboratory frame where an observer measures the spin wave period. As depicted in Fig. 4(a), at $t = 0$ the source, i.e., the exciting field in the middle of the film, emits a spin wave that is later detected by the observer at time $t = t_1 = x_0/v_\omega$ where x_0 is the distance the spin wave traveled at a velocity v_ω. The source accelerates to the right with acceleration a and emits a second spin wave at time $t = T$, this spin wave is detected at a time $t = t_2$. The spin-wave period as measured by the observer is $t_2 - t_1$ with t_2 given by the time between first and second emission T, plus the time it took the wave to travel a distance $x_0 - 1/2aT^2$ at a velocity v_ω,

$$t_2 - t_1 = T + \frac{x_0 - 1/2aT^2}{v_\omega} - \frac{x_0}{v_\omega} = T - \frac{aT^2}{2v_\omega}. \tag{13}$$

The frequency measured by the observer, $f_{ob} = 1/T_{ob} = 1/(t_2 - t_1)$ is expressed in terms of the proper frequency $f = 1/T$ as

$$f_{\text{obs}} = \frac{2f^2 v_\omega}{2f v_\omega - a}. \tag{14}$$

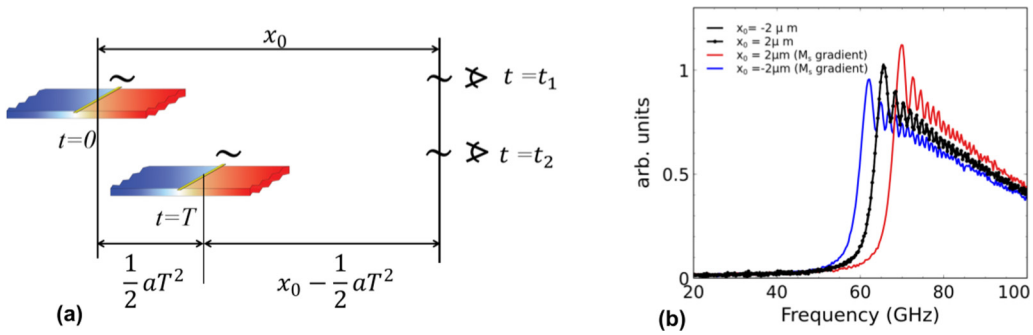

FIG. 4. Doppler effect. (a) Graphical description of the system of source and observer at times t_1 and t_2. (b) Frequency spectrum recorded at $x_0 = \pm 2\,\mu$m for the constant (black curves) and gradient (blue and red curves) cases.

To probe Eq. (14), we take $m_y(x,t)$, used to obtain the dispersion curves, and FFT it only along the temporal dimension into $m_y(x,f)$. In Fig. 4(b) we present the frequency spectrum registered at $x_0 = \pm 2\,\mu$m for the M_s gradient and the M_s constant cases. As expected, the frequency spectrum is identical for $x_0 = \pm 2\,\mu$m in the constant M_s case and corresponds to the proper-frequency spectrum. The M_s gradient case presents the same spectrum but shifted in frequency depending on whether the measurement was taken to the right at $x_0 = 2\,\mu$m or to the left at $x_0 = -2\,\mu$m of the source; this is due to the Doppler effect. As the source excites all frequencies up to 500 GHz, we focus on the peak of the spectrum to calculate the frequency shift with Eq. (14). We use the phase velocity $v_p = \omega_p/k_0$, corresponding to the frequency of the peak ω_p, to be the velocity of the wave, v_ω. With our parameters and considering the peak to be at $f = 65.7$ GHz, we get $f_{\text{obs}} = 66.3$ GHz when using $a = 7.52 \times 10^{11}$ m/s^2 computed above. The red peak in Fig. 4(b) found from simulations is at $f_{\text{obs}} = 69.8$ GHz so that the frequency shift is almost one order of magnitude larger than the calculated by the simplistic model given by Eq. (14). For a more accurate description, it would be necessary to discuss the approximations made throughout the derivation of our model.

D. Unidirectional propagation

The situation changes when instead of exciting in the middle of the film, the excitation is made at the edges of the film. We recorded the $m_y(x,t)$ component in response to field excitations of the same form as above but now placed at the edges of the film, $x = -8\mu$m and $x = 8\,\mu$m, and the same for the remaining magnetic parameters. The dispersion curve is presented in Fig 5(a). As we only record the magnetic component m_y within the gradient region, spin waves excited at the left edge $x = -8\,\mu$m, only propagate to the right. The $k > 0$ branch of the dispersion is delimited by the $M_s = 1.2$ MA/m and broadens to span the range of dispersions determined by the M_s values within the film. Similarly, spin waves excited at the right edge $x = 8\,\mu$m, propagate to the left, with the $k < 0$ branch bounded by the $M_s = 0.8$ MA/m dispersion curve and their dispersion broadens towards the dispersion for $M_s = 1.2$ MA/m. As a result, a discontinuity in the dispersion curve, shown in Fig. 5(a), is formed at $k = 0$ and creates a frequency gap between right and left propagating states that can be calculated as the difference between the ferromagnetic resonances of the delimiting dispersion curves,

$$\Delta\omega = \mu_0\gamma(M_s^- - M_s^+)\left(\frac{2K_u}{\mu_0 M_s^+ M_s^-} + 1\right), \qquad (15)$$

where $M_s^\pm$ corresponds to the delimiting M_s value for the positive or negative dispersion branch. With our parameters we find $\Delta f = \Delta\omega/2\pi = 37.5$ GHz. In our theoretical model, the situation is described by including $x_0 = \pm 8\,\mu$m in Eq. (5), which modifies the Airy wave packet by a shift in the argument of the Airy function and a modification of the phase by a factor $e^{\pm iB^2 t/(2\beta)Bx_0}$. Figure 5(b) shows the dispersion curve obtained from the theoretical model. The evident downward

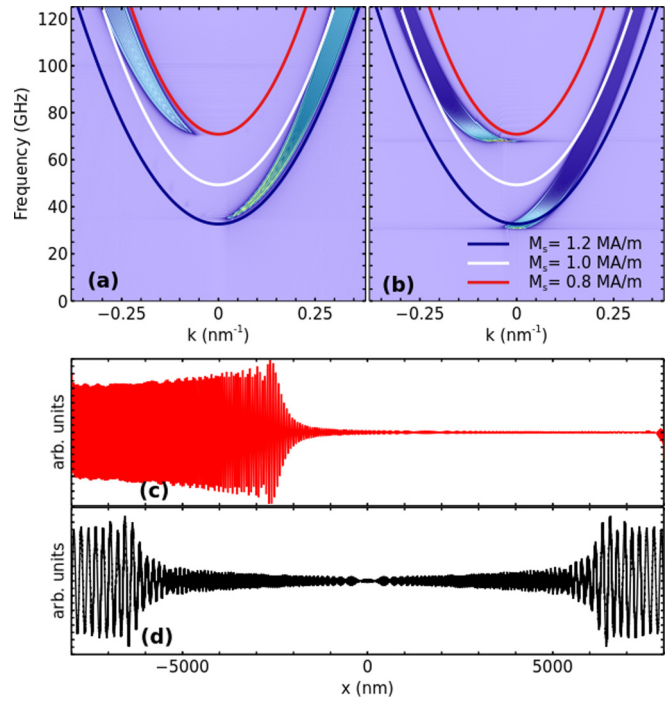

FIG. 5. Unidirectional propagation of spin waves. (a), (b) Dispersion curves found from micromagnetic simulations and theoretical model respectively where spin waves are excited at the edges of the M_s gradient region. A discontinuity is found near $k = 0$. Snapshot of the m_y component of the magnetization taken at $t = 3$ ns after the start of the excitation whereas in (c) a M_s gradient is considered and unidirectional propagation is achieved. For comparison (d) shows the constant M_s case where reciprocal propagation is exhibited.

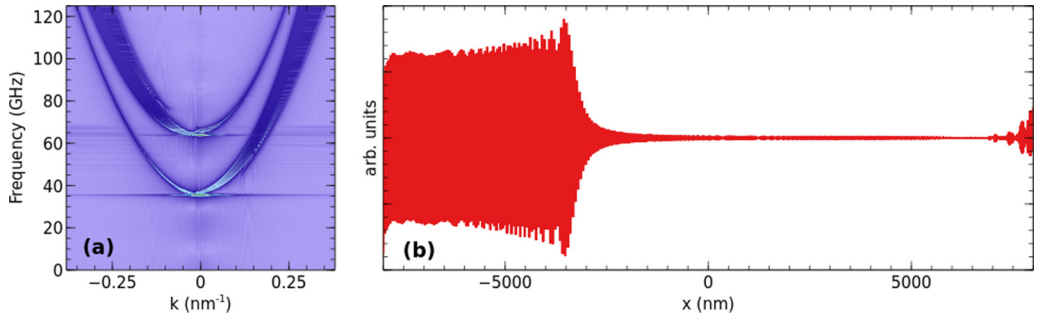

FIG. 6. Unidirectional propagation of spin waves. (a) Dispersion curves when the excitation sources are placed at $x_0 = \pm 6\,\mu$m. Both curves exhibit branches corresponding to $k > 0$ and $k < 0$. (b) Snapshot of the simulated spin waves at $t = 4$ ns in the case where the excitation is a sinusoidal field with frequency $f = 50$ GHz.

shift of the dispersion when compared to the simulation can be explained in terms of the neglected quadratic x term in the potential that becomes larger at the edges of the gradient region. A key consequence of the discontinuity is that within the gap only one direction of propagation is permitted depending on the sign of the M_s gradient. To verify, we again excite spin waves at the edges of the M_s gradient region but change the form of the excitation to a sinusoidal field $\mathbf{h}(t) = h_0 \sin(2\pi f t)\hat{\mathbf{y}}$ with $\mu_0 h_0 = 50$ mT and a fixed frequency $f = 50$ GHz, which is in the middle of the frequency gap. In Fig. 5(c) we present a snapshot taken at $t = 3$ ns: Propagation to the right is allowed while propagation to the left is forbidden. To compare, Fig. 5(d) shows what happens in the M_s homogeneous case where propagation is reciprocal. The situation presented above corresponds to the limiting case where the excitation is placed at the boundaries of the film. Experimentally, however, it may be challenging to place the excitation at the boundaries. We have repeated the simulation with the excitation sources now placed at $x_0 = \pm 6\ \mu$m, well within the film. The dispersion curve presented in Fig. 6(a) exhibits a gap at $k = 0$ whose magnitude is determined by Eq. (15) with $M_s^{\pm}$ corresponding to the saturation magnetization values at $x_0 = \pm 6\,\mu$m. Contrary to the limiting case, now the curves above and below the gap have branches $k > 0$ and $k < 0$. Still, when the excitation frequency is in the gap, the propagation is unidirectional as can be seen in Fig. 6(b) that shows a snapshot of the spin waves at $t = 4$ ns. As the excitation sources are placed closer together, the gap will decrease in magnitude and the propagation will become reciprocal.

III. CONCLUSIONS

Our results demonstrate that a M_s gradient induces a nonreciprocal propagation of spin waves in a perpendicularly magnetized ferromagnetic film. The M_s gradient is described by an additional linear potential as compared to the constant M_s case. Mathematically, the linear potential appears when transforming the constant M_s case to an accelerated reference frame with acceleration $-q/\beta$. The asymmetry in the dispersion is then explained as a Doppler effect. While nonreciprocity is observed in magnetostatic waves in thick films ($\approx$50 μm) [50,51], the non-reciprocity presented in this work can be achieved in films that are in the nanoscale in thickness. Finally, we demonstrate that unidirectional spin-wave propagation is achievable for a frequency band that depends on the M_s gradient extreme values. The unidirectional propagation phenomenon is highly dependent on the place of excitation as spin waves excited at the edges of the film can only propagate along one direction. However, even when the excitation source is placed within the film, the unidirectional propagation holds. As the excitation sources are placed together, the magnitude of the gap decreases and the propagation becomes reciprocal. An alternative system would consist of a film with a step function $M_s(x)$ such that M_{s1} is on the right-half side and M_{s2} on the left creating two available dispersion curves for propagation. The M_s gradient has two main advantages over the step function M_s, first the ability to dynamically control the gradient through a temperature landscape [35,36]. Second, a step function M_s would result in unwanted reflected and transmitted spin waves due to the discontinuity in M_s [37]. Unidirectional propagation of exchange spin waves is of the highest importance for the design of magnonic computing devices. Our results are given in terms of a M_s gradient that can be achievable through different methods, e.g., ion implantation [52–54]. However, the relevance of our study increases in light of recent studies in which modulation of the M_s parameter is realized via a thermal landscape. We used parameters that correspond to the expected variation of the saturation magnetization in a temperature range of 0–300 K in Pt/CoFeB. While the underlying physical mechanism is different, in practice, achieving unidirectional propagation by reversing the M_s gradient resembles the working principle of a diode. Lastly, we have also verified that our results hold in the case where M_s is constant throughout the film and the external magnetic field varies linearly.

Note added.—Recently, we became aware of work on similar effects through spatially varying exchange [55].

ACKNOWLEDGMENTS

This work was partially supported by Beca UNAM postdoctoral fellowship, Mitacs Globalink Research Award, National Council of Science and Technology of Mexico (CONACyT) under Project No. 253754 and CB A1-S-22695, PAPIIT IG100521, Natural Sciences and Engineering Research Council of Canada (NSERC)

APPENDIX: DERIVATION OF EQ (4).

We multiply Eq. (3) by M_s to get

$$iM_s\frac{\partial}{\partial t}m_+ = \gamma\left[-2A\frac{\partial^2}{\partial_x^2} + 2K_0 + \mu_0 H M_s\right]m_+ \tag{A1}$$

Now we substitute the spatial dependence of $M_s = M_0 + \alpha x$ together with the explicit definition of the effective anisotropy $K_0 = K_u - \mu_0 M_s^2/2$ to get

$$i(M_0+\alpha x)\frac{\partial}{\partial t}m_+ = \gamma\left[-2A\frac{\partial^2}{\partial_x^2} + 2K_u - \mu_0(M_0+\alpha x)^2 + \mu_0 H(M_0+\alpha x)\right]m_+, \tag{A2}$$

that can be rewritten as

$$iM_0\frac{\partial}{\partial t}m_+ = \gamma\left[-2A\frac{\partial^2}{\partial_x^2} + (2K_u - \mu_0 M_0^2 + \mu_0 H M_0) - \mu_0(\alpha x)^2 + \mu_0 H\alpha x - \mu_0 2M_0\alpha x - i\frac{\alpha x}{\gamma}\frac{\partial}{\partial_t}\right]m_+. \tag{A3}$$

Dividing by M_0 and defining $\omega_0 = \gamma(2K_0/M_0 + \mu_0 H - \mu_0 M_0)$, we obtain

$$i\frac{\partial}{\partial t}m_+ = \left[-\frac{2\gamma A}{M_0}\frac{\partial^2}{\partial_x^2} + \omega_0 - \frac{\gamma\mu_0}{M_0}(\alpha x)^2 + \frac{\gamma\mu_0\alpha x}{M_0}(H - 2M_0) - i\frac{\alpha x}{M_0}\frac{\partial}{\partial_t}\right]m_+, \tag{A4}$$

which corresponds to Eq. (4) when we define $qx = \gamma\mu_0\alpha(H - 2M_0)x/M_0$.

[1] J. Chen, C. Liu, T. Liu, Y. Xiao, K. Xia, G. E. Bauer, M. Wu, and H. Yu, Phys. Rev. Lett. **120**, 217202 (2018).

[2] A. V. Chumak, V. Vasyuchka, A. Serga, and B. Hillebrands, Nat. Phys. **11**, 453 (2015).

[3] G. Csaba, A. Papp, and W. Porod, Phys. Lett. A **381**, 1471 (2017).

[4] D. Grundler, Nat. Phys. **11**, 438 (2015).

[5] A. Khitun, M. Bao, and K. L. Wang, J. Phys. D: Appl. Phys. **43**, 264005 (2010).

[6] T. Schneider, A. A. Serga, B. Leven, B. Hillebrands, R. L. Stamps, and M. P. Kostylev, Appl. Phys. Lett. **92**, 022505 (2008).

[7] H. Yu, J. Xiao, and P. Pirro, J. Magn. Magn. Mater. Perspectives on magnon spintronics, **450**, 1 (2018).

[8] R. L. Stamps *et al.*, J. Phys. D **47**, 333001 (2014).

[9] A. V. Chumak and H. Schultheiss, J. Phys. D **50**, 300201 (2017).

[10] S. Neusser and D. Grundler, Adv. Mater **21**, 2927 (2009).

[11] V. V. Kruglyak, S. O. Demokritov, and D. Grundler, J. Phys. D: Appl. Phys. **43**, 264001 (2010).

[12] R. Vollmer, M. Etzkorn, P. S. A. Kumar, H. Ibach, and J. Kirschner, Phys. Rev. Lett. **91**, 147201 (2003).

[13] M. Etzkorn, P. S. A. Kumar, W. Tang, Y. Zhang, and J. Kirschner, Phys. Rev. B **72**, 184420 (2005).

[14] M. Plihal, D. L. Mills, and J. Kirschner, Phys. Rev. Lett. **82**, 2579 (1999).

[15] P. Che, K. Baumgaertl, A. Kúkol'ová, C. Dubs, and D. Grundler, Nat. Commun. **11**, 1445 (2020).

[16] S. J. Hämäläinen, F. Brandl, K. J. A. Franke, D. Grundler, and S. van Dijken, Phys. Rev. Appl. **8**, 014020 (2017).

[17] B. Heinz *et al.*, Nano Lett. **20**, 4220 (2020).

[18] C. Liu *et al.*, Nat. Commun. **9**, 738 (2018).

[19] F. Garcia-Sanchez, P. Borys, A. Vansteenkiste, J.-V. Kim, and R. L. Stamps, Phys. Rev. B **89**, 224408 (2014).

[20] M. Belmeguenai, J.-P. Adam, Y. Roussigné, S. Eimer, T. Devolder, J.-V. Kim, S. M. Cherif, A. Stashkevich, and A. Thiaville, Phys. Rev. B **91**, 180405(R) (2015).

[21] K. Di, V. L. Zhang, H. S. Lim, S. C. Ng, M. H. Kuok, X. Qiu, and H. Yang, Appl. Phys. Lett. **106**, 052403 (2015).

[22] J.-H. Moon, S.-M. Seo, K.-J. Lee, K.-W. Kim, J. Ryu, H.-W. Lee, R. D. McMichael, and M. D. Stiles, Phys. Rev. B **88**, 184404 (2013).

[23] F. J. dos Santos, M. dos Santos Dias, and S. Lounis, Phys. Rev. B **102**, 104401 (2020).

[24] K. Zakeri, Y. Zhang, J. Prokop, T.-H. Chuang, N. Sakr, W. X. Tang, and J. Kirschner, Phys. Rev. Lett. **104**, 137203 (2010).

[25] D. Cortés-Ortuño and P. Landeros, J. Phys.: Condens. Matter **25**, 156001 (2013).

[26] J. Chen *et al.*, Phys. Rev. B **100**, 104427 (2019).

[27] P. Grünberg, J. Appl. Phys. **57**, 3673 (1985).

[28] P. X. Zhang and W. Zinn, Phys. Rev. B **35**, 5219 (1987).

[29] M. Jamali, J. H. Kwon, S.-M. Seo, K.-J. Lee, and H. Yang, Sci. Rep **3**, 3160 (2013).

[30] C. S. Davies and V. V. Kruglyak, Low Temp. Phys. **41**, 760 (2015).

[31] C. S. Davies, A. Francis, A. V. Sadovnikov, S. V. Chertopalov, M. T. Bryan, S. V. Grishin, D. A. Allwood, Y. P. Sharaevskii, S. A. Nikitov, and V. V. Kruglyak, Phys. Rev. B **92**, 020408(R) (2015).

[32] H. Hata, T. Moriyama, K. Tanabe, K. Kobayashi, R. Matsumoto, S. Murakami, J.-I. Ohe, D. Chiba, and T. Ono, J. Magn. Soc. Jpn. **39**, 151 (2015).

[33] E. V. Tartakovskaya, A. S. Laurenson, and V. V. Kruglyak, Low Temp. Phys. **46**, 830 (2020).

[34] A. S. Laurenson, J. Bertolotti, and V. V. Kruglyak, Phys. Rev. B **102**, 054416 (2020).

[35] M. Vogel, R. Aßmann, P. Pirro, A. V. Chumak, B. Hillebrands, and G. von Freymann, Sci. Rep **8**, 11099 (2018).

[36] M. Vogel, A. V. Chumak, E. H. Waller, T. Langner, V. I. Vasyuchka, B. Hillebrands, and G. von Freymann, Nat. Phys. **11**, 487 (2015).
[37] P. Borys, N. Qureshi, C. Ordoñez-Romero, and O. Kolokoltsev, EPL **128**, 17003 (2019).
[38] S. Mieszczak, O. Busel, P. Gruszecki, A. N. Kuchko, J. W. Kłos, and M. Krawczyk, Phys. Rev. Appl. **13**, 054038 (2020).
[39] R. A. Gallardo, P. Alvarado-Seguel, T. Schneider, C. Gonzalez-Fuentes, A. Roldán-Molina, K. Lenz, J. Lindner, and P. Landeros, New J. Phys. **21**, 033026 (2019).
[40] O. Kolokoltsev, N. Qureshi, E. Mejía-Uriarte, and C. L. Ordóñez-Romero, J. Appl. Phys. **112**, 013902 (2012).
[41] A. Vansteenkiste, J. Leliaert, M. Dvornik, M. Helsen, F. Garcia-Sanchez, and B. Van Waeyenberge, AIP Advances **4**, 107133 (2014).
[42] Y. Zhou, R. Mansell, S. Valencia, F. Kronast, and S. van Dijken, Phys. Rev. B **101**, 054433 (2020).
[43] D. Kumar and A. O. Adeyeye, J. Phys. D: Appl. Phys. **50**, 343001 (2017).
[44] G. Venkat, D. Kumar, M. Franchin, O. Dmytriiev, M. Mruczkiewicz, H. Fangohr, A. Barman, M. Krawczyk, and A. Prabhakar, IEEE Trans. Magn. **49**, 524 (2013).
[45] J. Jorzick, S. O. Demokritov, B. Hillebrands, M. Bailleul, C. Fermon, K. Y. Guslienko, A. N. Slavin, D. V. Berkov, and N. L. Gorn, Phys. Rev. Lett. **88**, 047204 (2002).
[46] M. V. Berry and N. L. Balazs, Am. J. Phys **47**, 264 (1979).
[47] D. M. Greenberger and A. W. Overhauser, Rev. Mod. Phys. **51**, 43 (1979).
[48] D. M. Greenberger, Am. J. Phys **48**, 256 (1980).
[49] M. Feng, Phys. Rev. A **64**, 034101 (2001).
[50] J.-V. Kim, R. L. Stamps, and R. E. Camley, Phys. Rev. Lett. **117**, 197204 (2016).
[51] D. Stancil, *Spin Waves: Theory and Applications* (Springer, New York, 2009).
[52] D. Markó, T. Strache, K. Lenz, J. Fassbender, and R. Kaltofen, Appl. Phys. Lett **96**, 022503 (2010).
[53] D. McGrouther and J. Chapman, Appl. Phys. Lett **87**, 022507 (2005).
[54] J. Fassbender and J. McCord, J. Magn. Magn. Mater. **320**, 579 (2008).
[55] R. Macêdo, A. S. Kudinoor, K. L. Livesey, and R. E. Camley, arXiv:2012.10381.